Computers and Concrete, *Vol. 20, No. 4 (2017) 469-481*
DOI: https://doi.org/10.12989/cac.2017.20.4.469

Evaluation of interfacial shear stress in active steel tube-confined concrete columns

Mahdi Nematzadeh* and Jaber Ghadami[a]

Department of Civil Engineering, University of Mazandaran, Babolsar, Iran

(Received February 17, 2017, Revised April 25, 2017, Accepted April 27, 2017)

Abstract. This paper aims to analytically investigate the effect of shear stress at the concrete-steel interface on the mechanical behavior of the circular steel tube-confined concrete (STCC) stub columns with active and passive confinement subjected to axial compression. Nonlinear 3D finite element models divided into the four groups, i.e. circumferential-grooved, talc-coated, lubricated, and normal groups, with active and passive confinement were developed. An innovative method was used to simulate the actively-confined specimens, and then, the results of the finite element models were compared with those of the experiments previously conducted by the authors. It was revealed that both the predicted peak compressive strength and stress-strain curves have good agreement with the corresponding values measured for the confined columns. Then, the mechanical properties of the active and passive specimens such as the concrete-steel interaction, longitudinal and hoop stresses of the steel tube, confining pressure applied to the concrete core, and compressive stress-strain curves were analyzed. Furthermore, a parametric study was performed to explore the effects of the concrete compressive strength, steel tube diameter-to-wall thickness ratio, and prestressing level on the compressive behavior of the STCC columns. The results indicate that reducing or removing the interfacial shear stress in the active and passive specimens leads to an increase in the hoop stress and confining pressure, while the longitudinal stress along the steel tube height experiences a decrease. Moreover, prestressing via the presented method is capable of improving the compressive behavior of STCC columns.

Keywords: active confinement; bond shear stress; composite column; finite element modeling; mechanical behavior; numerical analysis; STCC

1. Introduction

Steel tube-confined concrete (STCC) columns have become increasingly popular in various structural applications like bridge piers, high-rise building columns, arch centering, and large industrial workshops due to their excellent properties such as high ductility, resistance and stiffness against earthquakes, and perfect composite action between the concrete core and steel tube (Qi *et al.* 2011). One of the main parameters affecting the behavior of STCC columns is the shear stresses due to the friction at the interface between the concrete core and steel tube, which generate longitudinal compressive stresses in the steel tube, causing the steel tube to reach the yield point at a lower hoop tensile stress, and the confinement pressure applied to the concrete core to decrease. Generally, concrete confinement can be either active or passive; the latter of which involves no lateral pressure to the concrete core prior to loading, while in the former, a lateral pressure is applied to the concrete core, prior to loading. Prestressing the composite columns is performed in various ways; one of which is the active confinement of fresh concrete first developed by Nemati (2006) and then investigated extensively by Nematzadeh *et al.* (2017).

It is well known that conducting full-scale experiments is a more efficient way to understand the structural members' behavior; however, experimental studies with large specimen size and number are both costly and time-consuming. This leads to the employment of numerical methods for performing parametric studies. One of the most widely used numerical methods is the finite element method (FEM) which has been receiving significant attention in the last few decades for predicting the behavior of STCC and concrete-filled steel tube (CFST) columns due to the availability of many commercial software programs such as the ABAQUS and ANSYS (Yu *et al.* 2010, Shraideh and Aboutaha 2013, Gupta *et al.* 2015). Finite element analysis (FEA) allows for a direct modeling of the composite action between steel and concrete components, and a more accurate consideration of various factors including local and global imperfections, residual stresses, and boundary conditions. Nevertheless, the prediction accuracy offered by a finite element model is greatly affected by the input parameters and, in particular, the choice of an appropriate model for the concrete (Tao *et al.* 2013).

Schneider (1998) developed a 3D nonlinear finite element model using the ABAQUS program to model the circular CFST columns, and employed the unconfined uniaxial stress-strain curve of the concrete material available in the ABAQUS material library. Comparing the finite element analysis results with those of the experiments showed that both of the obtained behaviors are very similar

*Corresponding author, Assistant Professor
E-mail: m.nematzadeh@umz.ac.ir
[a]Graduate Student

ISSN: 1598-8198 (Print), 1598-818X (Online)

Table 1 Mechanical and geometric properties of the composite section components

Specimen ID	Type of confinement	Type of concrete	Concrete compressive strength (MPa)	L_c (mm)	L_s (mm)	D/t	t (mm)	ε_h ($\mu\varepsilon$)	E_s (GPa)	f_y (MPa)	f_u (MPa)
CPC	Passive	normal	30.8	140	150	24.2	2.5	-	210	339	480
LPC	Passive	normal	30.8	140	150	24.2	2.5	-	210	339	480
TPC	Passive	normal	30.8	140	150	24.2	2.5	-	210	339	480
NPC	Passive	normal	30.8	140	150	24.2	2.5	-	210	339	480
CAC	Active	compressed	66.7	124	134	24.2	2.5	464	210	339	480
LAC	Active	compressed	66.7	124	134	24.2	2.5	464	210	339	480
TAC	Active	compressed	66.7	124	134	24.2	2.5	464	210	339	480
NAC	Active	compressed	66.7	124	134	24.2	2.5	464	210	339	480

in the elastic and plastic stages. Hu *et al.* (2003) developed a nonlinear finite element model using the ABAQUS program in order to simulate the behavior of CFST columns. Through a parametric study and via matching the numerical results with the experimental ones, they proposed empirical equations for the confining pressure and the material degradation parameter, which were a function of the diameter-to-wall thickness ratio and the yield stress of the steel tube. Tao *et al.* (2013) performed the finite element modeling of the concrete-filled stub columns under axial compression. They gathered a large collection of experimental data which was then used to develop refined FE (finite element) models to simulate CFST stub columns under axial compressive loading, and they also proposed a new strain hardening/softening function for the confined concrete, in which no confinement-induced increase in strength was considered. In addition, new expressions for the material parameters available in the concrete damage plasticity model were proposed, which were defined as a function of the unconfined concrete compressive strength and the confinement factor. Johansson and Gylltoft (2002) performed an experimental and analytical study on the mechanical behavior of the circular concrete-steel composite stub columns under three axial loading conditions, and the finite element results of the study demonstrated that when axial loading is applied only to the concrete core, the structural behavior and the effect of confinement on the concrete core are significantly affected by the bond strength at the concrete-steel interface, while in the case where axial loading is applied to the entire column cross-section, the bond strength has no influence on the structural behavior. Furthermore, as the concrete-steel bond strength increases, so does the stiffness of the STCC columns.

In spite of the fact that numerous numerical studies have been carried out on the behavior of the columns with passive confinement so far, the literature includes very few studies concerning modeling the columns with active confinement. In this regard, Haghinejad and Nematzadeh (2016) and Nematzadeh and Haghinejad (2017) performed studies on modeling of the STCC columns having passive and active confinement, respectively, in which they proposed a new stress-strain model for the confined concrete in the passive and active confinement by matching the FEM results with the experimental ones. Chen and Andrawes (2012) put forward a plasticity model to predict the behavior of the concrete confined with shape memory alloy (SMA) under a monotonic compression, in which the hardening/softening function and flow rule were represented based on the lateral confining pressure, confinement type, and plastic deformation. The FE analysis of the SMA-confined concrete showed a good consistency with the experimental results. In the work of Moghadam *et al.* (2010), the nonlinear finite element analysis method was employed using the Lubliner damage plasticity model to analyze the compressive behavior of the concrete confined with external closed post-tensioned strips. By utilizing the values given for the various parameters introduced in the study, the proposed method was capable of logically estimating the compressive behavior of the tested specimens.

The main goal of the present study is to conduct the finite element modeling of the active and passive STCC columns in order to investigate the effect the shear stress at the concrete core-steel tube interface has on the compressive behavior of these columns. The finite element computer program ABAQUS (2003) is used for the 3D nonlinear analysis of the composite columns, in which an innovative method is presented to model the actively-confined specimens. The results obtained from the finite element model are compared with the experimental results previously reported by Ghadami and Nematzadeh (2016) in the four groups of the circumferential-grooved, lubricated, talc-coated, and normal specimens. After the verification of the model, the effect of various interface shear stress conditions on mechanical properties of the specimens subjected to axial compression is explored. Finally, a parametric study is conducted to investigate the effect of concrete strength, steel tube diameter-to-wall thickness ratio, and prestressing level on the compressive behavior of the actively- and passively-confined STCC columns.

2. Summary of the experimental investigation

The experimental study performed by Ghadami and Nematzadeh (2016) involved the effect the concrete-steel interface shear stress had on the compressive behavior of the STCC columns with active and passive confinement. A summary of the experimental procedure is described here. The steel tubes used in the study were all seamless tubes produced via hot forming, with the outer diameter (D) and wall thickness (t) of 60.5 and 2.5 mm, respectively. The tube height (L_s) in the active and passive specimens was 134 and 150 mm, respectively, with the concrete height (L_c) being 124 and 140 mm, respectively. The geometry and mechanical properties of the steel tubes are summarized in Table 1, where f_y, f_u, and E_s are yield strength, ultimate strength, and initial modulus of elasticity of the steel, respectively.

In total, 24 confined concrete specimens, of which half were actively confined and the other half were passively confined, were made in the lab. STCC columns with passive and active confinement were divided into four groups including; (1) circumferential-grooved specimens

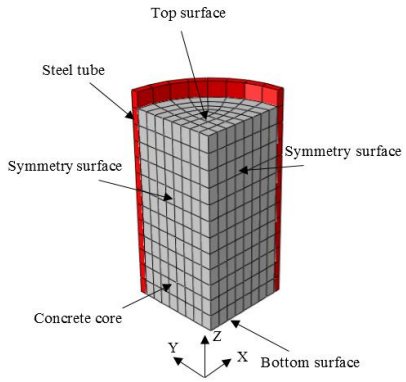

(a) Boundary conditions and mesh for one-eighth of the STCC column

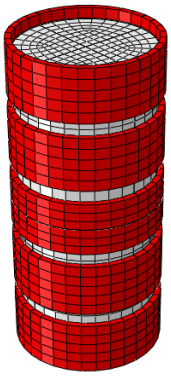

(b) A full model of the grooved specimen

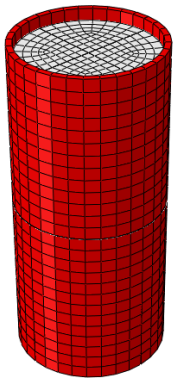

(c) A full model of the lubricated, talc-coated, and normal specimens

Fig. 1 A schematic view of the geometry, boundary conditions, and mesh of the specimens

(C), (2) lubricated specimens (L), (3) talc-coated specimens (T), and (4) normal specimens (N) (without being circumferential-grooved, talc-coated, and lubricated). The grouping was performed in order to investigate the effect of the concrete-steel interface shear stress on the two confinement types (active and passive) under axial loading. In the circumferential-grooved specimens, the steel tube was cut into five rings, so that the mean groove width of active and passive specimens was 5.87 and 6.9 mm, respectively. In the case of the talc-coated specimens, the thickness of talc coating used was 0.13 mm. The compressive strength of uncompressed and compressed concrete in all the active and passive specimens was 30.8 and 66.7 MPa, respectively.

To prestress the confined concretes, an axial pressure was applied to the fresh concrete for 12 days. Twelve concrete-filled steel tubes were placed successively in the pressure device in which the specimens were separated by circular rigid steel plates (for more details on the pressure device, see Nematzadeh and Naghipour 2012). In this prestressing method, by applying pressure to the fresh concrete inside the steel tubes, not only the concrete is compressed, but also the steel tube is pre-tensioned laterally. The level of prestressing was measured by horizontal strain gauges mounted at the mid-height of the steel tubes on the outer wall, with the mean value of 464 microstrain measured for the amount of the ultimate hoop strain (ε_h) being equivalent to the lateral pressure of 8.78 MPa applied to the concrete core. The characteristics of the actively-confined specimens belonging to the four groups of circumferential-grooved (CAC), lubricated (LAC), talc-coated (TAC), and normal (NAC) specimens together with those of the passively-confined specimens in the four groups of circumferential-grooved (CPC), lubricated (LPC), talc-coated (TPC), and normal (NPC) specimens are presented in Table 1.

After the passage of a 28-day curing time from the date of casting concrete, the confined specimens were subjected to axial compression by a compression testing machine.

3. Finite element modeling

3.1 General

The ABAQUS software was employed in this study in order to model the steel tube-confined concrete columns with the two confinement types of active and passive each consisting of four groups, i.e., circumferential-grooved, talc-coated, lubricated, and normal specimens. Constructing the model was carried out in three steps; concrete core modeling in the active and passive specimens, steel tube modeling, and concrete core-steel tube interaction modeling. Various parameters applied in the modeling of the passive specimens in the ABAQUS were adopted from the results reported by Haghinejad and Nematzadeh (2016). Moreover, a new method first proposed by Nematzadeh and Haghinejad (2017) was used in the modeling of the active specimens.

3.2 Element type and mesh

Both the steel tube and the concrete core of the STCC specimens were modeled using 8-node brick elements (C3D8R), with three translational degrees of freedom at each node. In addition, different mesh sizes were used to obtain a mesh with acceptable results and shorter computation time. It was found that the mesh shown in Fig. 1 gives accurate results as well as logical computation time.

3.3 Boundary conditions and loading

Given the symmetry, only 1/8 of the circular STCC columns was modeled, as shown in Fig. 1. The top surface of the columns is restrained against all degrees of freedom except the displacement along the Z-axis; however, the

model's bottom surface (mid-height of the columns) is restrained along the Z-axis while being free in other directions. As can be seen in Fig. 1, due to symmetry, the displacement of the nodes of the symmetrical Y-Z and X-Z planes is restrained along the X- and Y-axis, respectively, while the other nodes are free to move in any direction.

In the passive specimens, the loading is applied as uniform static loads based on the displacement control of each node at the loading surface (the top surface of the concrete core) in order to obtain similar conditions to the experimental study. Due to prestressing, loading the active specimens is performed in three steps; the first of which involves the application of a uniform compressive load to the steel tube inner wall. In this step, the diameter of the steel tube is considered a little smaller than the diameter of the concrete core; hence no concrete-steel interaction is defined. In addition, the amount of lateral pressure must be considered such that the steel tube inner wall be able to detach from the concrete core provided that the steel tube remains within the elastic range. The existence of an initial distance between the steel tube and concrete core in this loading step is to apply prestressing to the active specimens, and the amount of this distance depends on the prestressing level of the specimens.

In the second loading step where an interaction is defined between the concrete and steel, the lateral pressure applied to the inner wall of the steel tube is removed, and since the steel tube is still within the elastic range, it tends to return to the initial condition. However, the concrete core intervenes as the steel tube is returning to its initial condition, thus the steel tube becomes restrained. Once the steel tube inner wall makes contact with the concrete core and regarding the interaction present between the two in this step, the concrete experiences lateral pressure. Notice that at the end of the second step which marks the beginning of the axial loading, the amount of lateral pressure applied to the concrete core should be equal to the prestressing level of the active specimen. In other words, the steel tube hoop strain of the model at the end of the second step should be equal to that of the experiments at the beginning of the compression tests. This objective is accomplished in this research by changing the inner diameter of steel tube prior to the application of axial loading (the third loading step), and by using trial and error method. Note that until the model prestressing level becomes equal to the experimental one (which means the verification of the first and second loading steps), the third step would not start; in other words, the first and second loading steps are the prerequisites of the third one. Lateral loading and unloading at the first and second loading steps are performed by defining an appropriate amplitude which is actually a history of the given loading.

In the third loading step, by utilizing the General Static Analysis method available in the ABAQUS library, a uniform static load is applied to the nodes located at the top surface of the concrete core with the displacement-controlled load; to be consistent with the experimental studies.

3.4 Modeling the concrete materials

3.4.1 Modeling the passively-confined concrete

The equivalent uniaxial stress-strain curve of concrete with passive confinement together with that of the unconfined concrete is plotted in Fig. 2(a), in which f_c is the cylindrical compressive strength of the unconfined concrete. The strain at peak stress (ε_c) of the unconfined concrete is 0.003, as specified by the ACI Code (2008), and the compressive strength of the passively-confined concrete (f_{pc}) and its corresponding strain (ε_{pc}) can be calculated by Eqs. (1)-(2), respectively (Mander *et al.* 1988),

$$f_{pc} = f_c + k_1 f_l \tag{1}$$

$$\varepsilon_{pc} = \varepsilon_c \left(1 + k_2 \frac{f_l}{f_c}\right) \tag{2}$$

where f_1 is the lateral confining pressure applied to the concrete by the steel tube. Based on the empirical equations obtained by matching the modeling and experimental results of the passive STCC columns, the value of f_1 is proposed as Eq. (3) (Haghinejad and Nematzadeh 2016).

$$\frac{f_l}{f_y} = 0.034366 - 0.000452\left(\frac{D}{t}\right) \tag{3}$$

In accordance with the results of the experiments performed by Richart *et al.* (1928) on the fluid-confined specimens, k_1=4.1 and k_2=5k_1 are considered. It should be noted that no shear stress exists in a fluid; however, when the STCC column undergoes axial compression, the concrete core displacement in the longitudinal direction is prevented by the steel tube inner wall, leading to the development of shear stresses at their interface. These shear stresses give rise to compressive stresses along the length of the steel tube resulting in a reduction of the confinement effect, and thus a change in k_1 and k_2 factors is followed. In the current study, regarding the equation proposed by Nematzadeh *et al.* (2017) for the STCC columns, the factor k_1 is taken as 2.17 for the passive normal specimens and 4.1 for the passive talc-coated and circumferential-grooved specimens. For all passive specimens, the factor k_2 is considered five times as much as the value of factor k_1. The increase from 2.17 to 4.1 in the passive talc-coated and circumferential-grooved specimens is due to the significant portion of the steel tube confinement caused by the elimination or reduction of the interface shear stress and the longitudinal stress, which leads to a greater confinement effectiveness coefficient. By knowing the values of f_1, k_1, and k_2, Eqs. (1)-(2) gives the values of f_{pc} and ε_{pc}, respectively.

To define the equivalent uniaxial stress-strain curve of the passively-confined concrete, as shown in Fig. 2(a), three regions of the curve have to be identified; the first of which is the linear elastic region ranging from the origin to the proportional limit stress which is taken as with respect to 0.5f_{pc} the work of Hu *et al.* (2003). In order to define the elastic region of the concrete material in the ABAQUS, the initial modulus of elasticity of the passively-confined concrete (E_{pc}) is obtained by the empirical Eq. (4) given by ACI (2008), and its Poisson's ratio (ν_{cc}) is taken as 0.2.

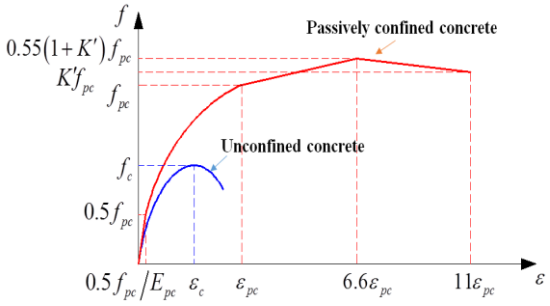

(a) Passively-confined concrete along with the unconfined concrete

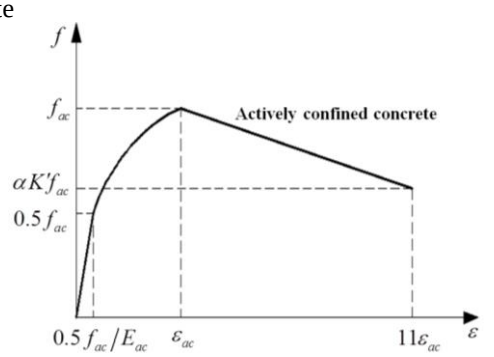

(b) Actively-confined concrete

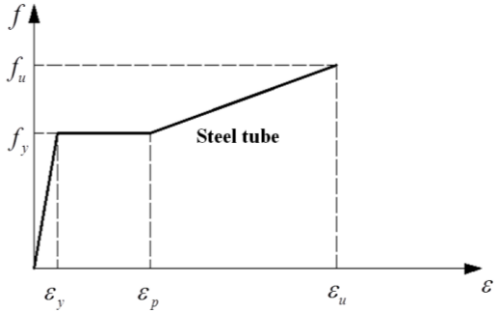

(c) Steel

Fig. 2 The equivalent uniaxial stress-strain curve

$$E_{pc} = 4730\sqrt{f_{pc}} \quad \text{MPa} \tag{4}$$

The second region of the stress-strain curve is the nonlinear region starting from the proportional limit stress, $0.5f_{pc}$, along with its corresponding strain, $0.5f_{pc}/E_{pc}$, and continuing to the passively-confined concrete strength, f_{pc}, with its corresponding strain of ε_{pc}. This region of the curve is obtained by Eq. (5) proposed by Saenz (1964). For this region of the curve, the uniaxial stress (f) in terms of the uniaxial strain (ε) is calculated from the following equation,

$$f = \frac{E_{pc}\varepsilon}{1+(R+R_E-2)\left(\frac{\varepsilon}{\varepsilon_{pc}}\right)-(2R-1)\left(\frac{\varepsilon}{\varepsilon_{pc}}\right)^2+R\left(\frac{\varepsilon}{\varepsilon_{pc}}\right)^3} \tag{5}$$

where R_E and R are the modular ratio and ratio relation, respectively, given by Eqs. (6)-(7).

$$R_E = \frac{E_{pc}\varepsilon_{pc}}{f_{pc}} \tag{6}$$

$$R = \frac{R_E(R_\sigma - 1)}{(R_\varepsilon - 1)^2} - \frac{1}{R_\varepsilon} \tag{7}$$

The constants R_σ and R_ε are the stress ratio and strain ratio, respectively, both taken as 4 as suggested by Hu and Schnobrich (1989).

The third region of the confined concrete stress-strain curve consists of two lines; the first of which starts from the passively-confined concrete strength, f_{pc}, and proceeds to the strength of $0.55f_{pc}(1+K')$ with the corresponding strain of $6.6\varepsilon_{pc}$. The second line is a descending line spanning from the end of the previous line to the ultimate strength of $K'f_{pc}$ with the corresponding strain of $11\varepsilon_{pc}$. K' is a coefficient obtained by the expressions given in Eq. (8) (Haghinejad and Nematzadeh 2016).

$$K' = \begin{cases} \left(0.0264865 - 0.0003861\dfrac{D}{t}\right)(85 - 0.625f_c) \\ 24.2 \le \dfrac{D}{t} \le 29.75,\ 16.7 \le f_c \le 52.6 \\ \left(0.0169283 - 0.0000662\dfrac{D}{t}\right)(85 - 0.625f_c) \\ 29.75 < \dfrac{D}{t} \le 57.5,\ 16.7 < f_c \le 52.6 \end{cases} \tag{8}$$

3.4.2 Modeling the actively-confined concrete

In the present prestressing method, via compressing the fresh concrete inside the steel tube by the prestressing apparatus, the concrete core not only becomes prestressed but also turns into a compact material; hence, the concrete core in these specimens exhibits different behavior from that of the passively-confined specimens. Fig. 2(b) shows the equivalent uniaxial stress-strain curve of the concrete with active confinement. The compressive strength of the actively-confined concrete (f_{ac}) as well as its corresponding strain (ε_{ac}) can be calculated from Eqs. (9)-(10), respectively, developed by Nematzadeh *et al.* (2017) based on the experimental results of the active STCC specimens.

$$f_{ac} = \left(2.31\left(\frac{f_l}{f_{uc}}\right)^{0.7}(1+P_r)f_{uc}\right) + f_{uc} \tag{9}$$

$$\varepsilon_{ac} = \left(5\left(\frac{f_{ac}}{f_{uc}} - 1\right) + 1\right)\varepsilon_c \tag{10}$$

In the above equations, f_{uc} is the compressive strength of the unconfined compressed concrete given by the following equation (Nematzadeh and Naghipour 2012),

$$f_{uc} = -0.0331f_c^{\,2} + 3.185f_c \ \text{MPa} \tag{11}$$

Also, P_r is the prestressing ratio of the actively-confined concrete defined as

$$P_r = \frac{P_f}{f_{uc}} \tag{12}$$

in which P_f is the prestressing level or, in other words, the amount of ultimate lateral pressure applied to the concrete core. The prestressing level of the active specimens can be expressed in terms of the steel tube hoop strain by the following equation

$$P_f = \frac{2t\, E_s\, \varepsilon_h}{D_i} \quad (13)$$

where D_i denotes the steel tube inner diameter. In Eq. (9), the factor of 2.31 is introduced for the active normal concrete specimens, which is increased to 4.36 and 5.85 for the active circumferential-grooved and talc-coated specimens, respectively, due to fact that the confinement contribution in these specimens increases as a result of reduction or elimination of the concrete-steel interface shear stress, as previously discussed for the confinement effectiveness coefficient in the passive specimens.

A new 3-stage model is proposed in order to capture the stress-strain curve of actively-confined concrete, as shown in Fig. 2(b). The first stage is the elastic region considered up to the proportional limit stress, $0.5f_{ac}$. The initial modulus of elasticity of the actively-confined concrete (E_{ac}) is determined by the empirical equation (Eq. (14)) developed by Nematzadeh and Naghipour (2012) written as follows

$$E_{ac} = 3496.5\sqrt{f_{uc}} + 15932 \ \text{MPa} \quad (14)$$

The second stage is the nonlinear region before the peak point is reached that is similar to that of the passively-confined concrete, and the third stage is the descending linear region following the peak point starting from the peak strength, f_{ac}, and continuing to the ultimate stress, $\alpha K' f_{ac}$, for which α is the conversion factor of the passive curve to the active one taken in this paper as 0.9 (Nematzadeh and Haghinejad 2017).

3.4.3 Concrete yield surface

Since this paper only investigates STCC stub columns under monotonic loading, damage variables are not defined; hence, only the nonlinear region of concrete is defined as the plastic mode. The yield region of the confined concrete stress-strain curve, which occurs after the proportional limit stress, is modeled utilizing the Drucker-Prager yield criterion model which is available in the ABAQUS material library. In this model, the yield surface and flow potential parameters are defined using the two options of "DRUCKER PRAGER" and "DRUCKER PRAGER HARDENING" in the yielding stage of the confined concrete. The parameters present in this model include internal friction angle of materials (β), ratio of the flow stress in triaxial tension to that in triaxial compression (K), and dilation angle (ψ). The values of internal friction angle and flow stress ratio for the actively- and passively-confined concretes in all the normal, lubricated, talc-coated, and circumferential-grooved specimens are considered as 20 degrees and 0.8, respectively. The concrete dilation angle, ψ, is a function of volume changes during shear loading, with a brittle behavior resulting from a small value of ψ while a higher value of ψ leads to a more ductile behavior. Since the value of ψ affects the compressive hardening of concrete, choosing an appropriate value for which is essential for accurate simulation of the behavior of the concrete materials. In the ABAQUS, the allowed value of ψ for the confined concrete ranges from 0 to 56 degrees (Tao *et al.* 2013). In the present work, ψ for the actively- and passively-confined concrete in the normal and lubricated specimens is taken as 35 degrees, and in the circumferential-grooved and talc-coated specimens, it is considered as 20 and 15 degrees, respectively. Regarding the small lateral deformation (dilation) of the concrete in the talc-coated and circumferential-grooved specimens, a smaller dilation angle compared to that of the normal specimen is required.

3.5 Modeling the steel material

Here, the trilinear stress-strain curve is used for the modeling of steel tube, as can be seen in Fig. 2(c). By employing the "PLASTIC" option in the ABAQUS, the plastic behavior of materials can be captured, which allows for the use of a multi-linear stress-strain curve for steel tubes. Yield strain, ε_y, strain at the onset of strain hardening, ε_p, and ultimate strain, ε_u, of the steel are 0.0016, 0.0139, and 0.114, respectively, adopted from the experimental data reported by Ghadami and Nematzadeh (2016). Furthermore, the steel yield and ultimate strength (f_y and f_u) are 339 and 480 MPa, respectively. The first part of the curve from the origin to the yield stress demonstrates the elastic region defined by taking the modulus of elasticity and Poisson's ratio of steel as 210 GPa and 0.28, respectively.

3.6 Steel-concrete interface model

The interface model capable of simulating the interaction between the steel and concrete in the STCC specimens is the contact interaction in the ABAQUS, which can mechanically simulate two deformable bodies at the interface. Contact interaction is defined with two aspects: geometric property and mechanical property. The geometric property of contact surfaces is defined by the proper selection of contact discretization and tracking approach, as well as by determining the master and slave surfaces. Surface-to-surface contact is usually used for the interaction simulation of the steel tube and concrete core in the ABAQUS. This method requires the definition of the two surfaces termed as the master and slave surfaces; the inner surface of the steel tube is considered as the master surface while the outer surface of the concrete core is taken as the slave surface in this model. Furthermore, a finite sliding tracking approach has been chosen for the steel-concrete contact surfaces. This approach is more effective for STCC columns where there is a sliding between the concrete and steel surfaces. In order to define the mechanical property of contact surfaces, the contact interaction is defined by the two normal and tangential behaviors. The "hard contact" option in the normal contact is specified for the interface, which allows the separation of the interface in tension while no penetration can occur in it in compression. The tangential contact is simulated using Coulomb friction model, and the penalty method is used to formulate the tangential friction behavior. In this work, the friction

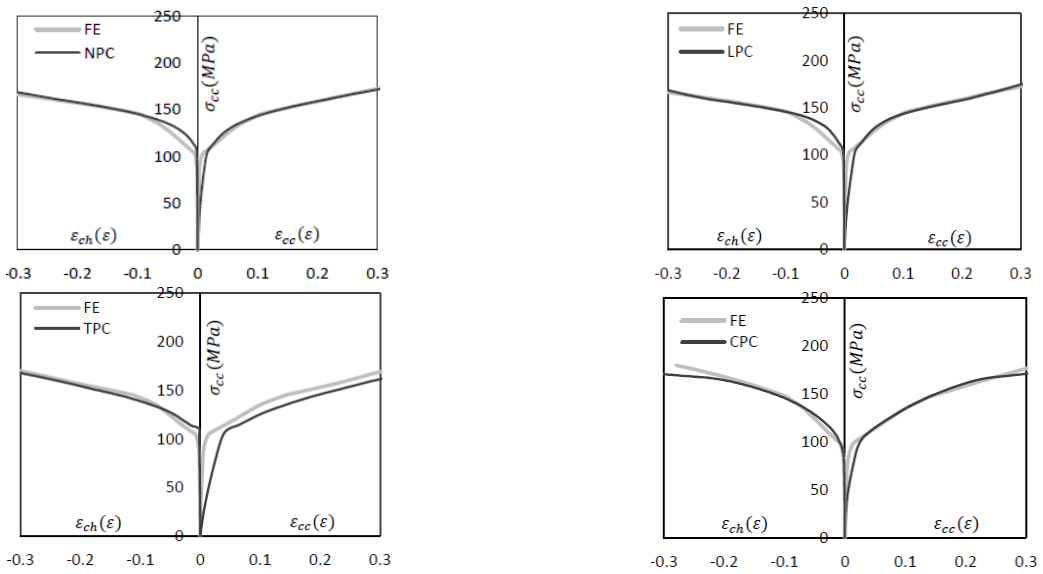

(a) Passively-confined specimens

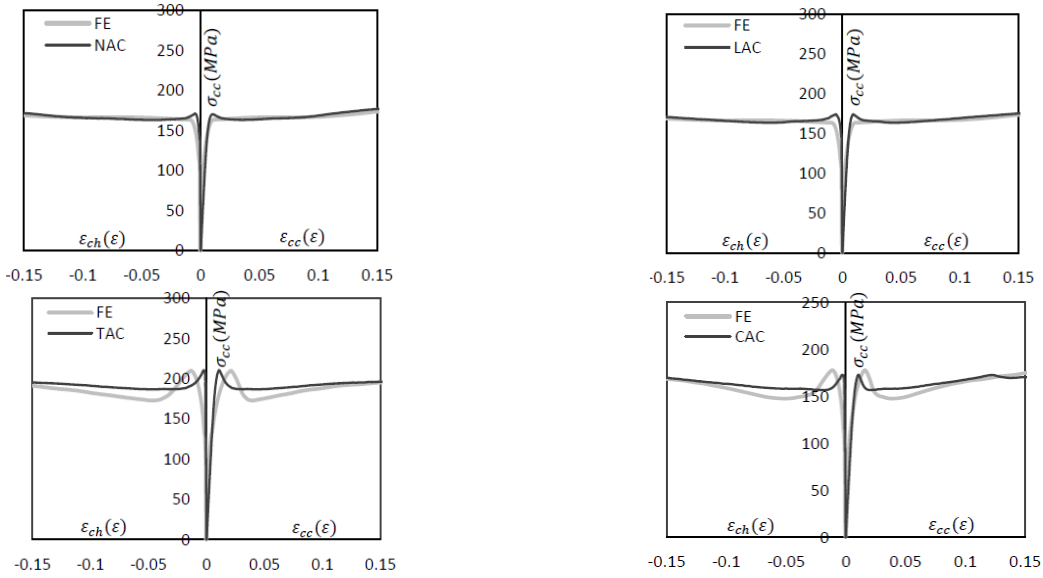

(b) Actively-confined specimens

Fig. 3 Comparison between the numerical and experimental stress-strain curves for the actively- and passively-confined specimens

Table 2 The experimental and FEA results of the actively- and passively-confined specimens

Specimen ID	Type of confinement	$f_{cc(Test)}$ (MPa)	$f_{cc(FE)}$ (MPa)	$f_{cc(Test)}/f_{cc(FE)}$
CPC	Passive	106.7	100.8	1.06
LPC	Passive	111.6	106.5	1.05
TPC	Passive	109.1	106.8	1.02
NPC	Passive	109.8	106.5	1.03
CAC	Active	168.1	177.9	0.95
LAC	Active	177.9	163.3	1.09
TAC	Active	218.7	209.8	1.04
NAC	Active	170.3	163.3	1.04

coefficient between the two surfaces is considered as 0.65 for the normal, lubricated, and circumferential-grooved specimens. In addition, no friction is defined between the contact surfaces of the concrete core and steel tube in talc-coated specimens.

4. Verification of the finite element model

In order to verify the analysis accuracy, the finite element results of the STCC specimens are compared with the experimental results of Ghadami and Nematzadeh (2016) in terms of the peak compressive strength and stress-strain curves. In Fig. 3, the model-predicted and experiment-measured axial stress vs. axial strain (σ_{cc}-ε_{cc}) and lateral strain (σ_{cc}-ε_{ch}) curves for the circumferential-grooved, lubricated, talc-coated, and normal specimens with active and passive confinement are given for comparison. It is understood from Fig. 3 that there is a good agreement

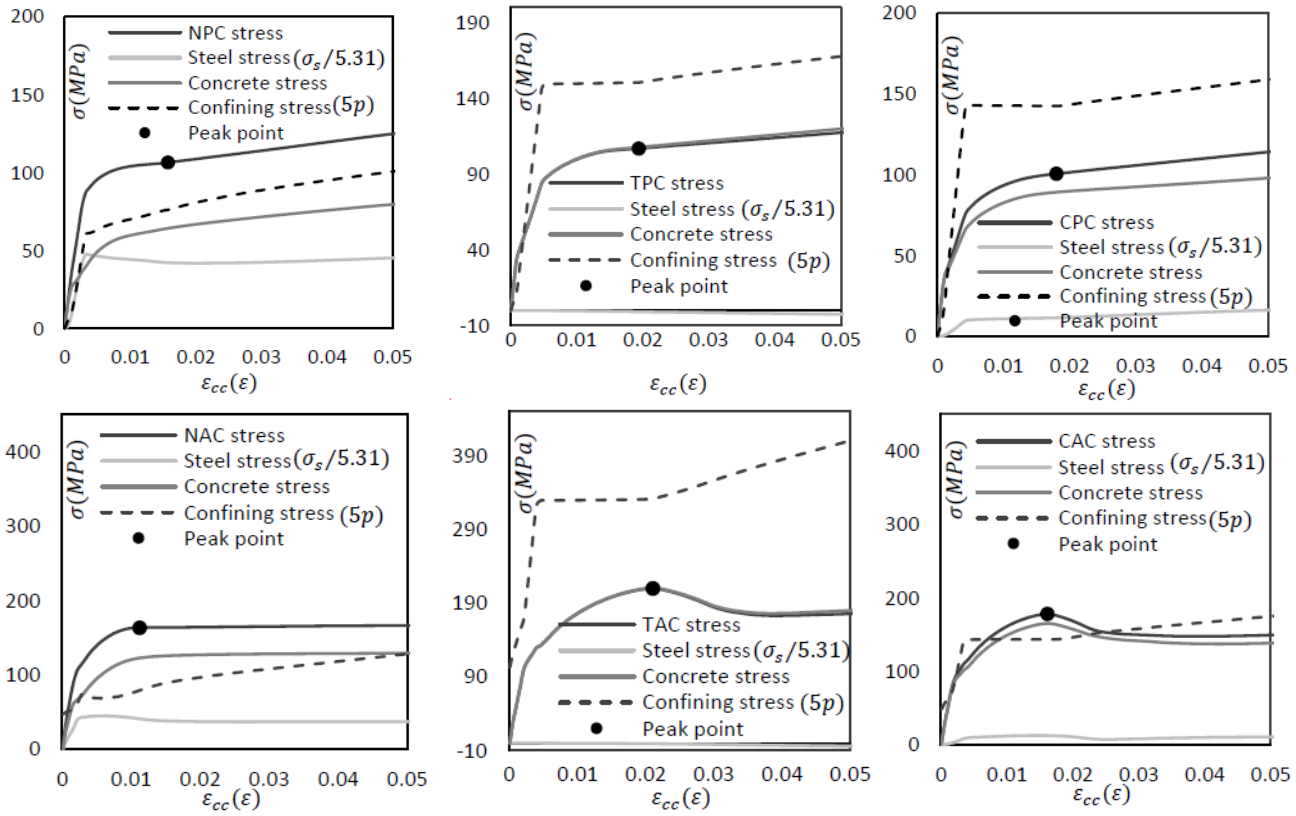

Fig. 4 The stress-strain curves of composite section components along with the confining stress

between the experimental and FEA results. Table 2 gives the values of the peak compressive strength obtained from the tests ($f_{cc(TEST)}$) together with those predicted by the finite element model ($f_{cc(FE)}$) for active and passive specimens. Here, the peak compressive strength in the active specimens is the compressive strength corresponding to the relative maximum stress in the stress-strain curve. Also, in the passive specimens, due to the absence of a relative maximum value for stress, the peak compressive strength corresponds to the starting point of the steel strain hardening, which is a point in the stress-strain curve where the convexity of the curve (curvature sign) changes, i.e., curve inflection point. With respect to Table 2, the $f_{cc(TEST)}/f_{cc(FE)}$ ratio for the actively- and passively-confined specimens in the circumferential-grooved, lubricated, talc-coated, and normal groups is about 1. Hence, the above comparisons reveal the good agreement of the experimental and FEA results.

5. Finite element model results

5.1 Load-carrying portion of the composite section components

The axial stress vs. axial strain curves for each of the composite section components along with the confining stress (p) vs. axial strain curves at the mid-height of the active and passive composite columns are shown in Fig. 4, in which the axial stress (σ_s) curves of the steel tube and the confining stress curves are divided by 5.31 (=concrete to steel cross-section ratio) and multiplied by 5, respectively. It

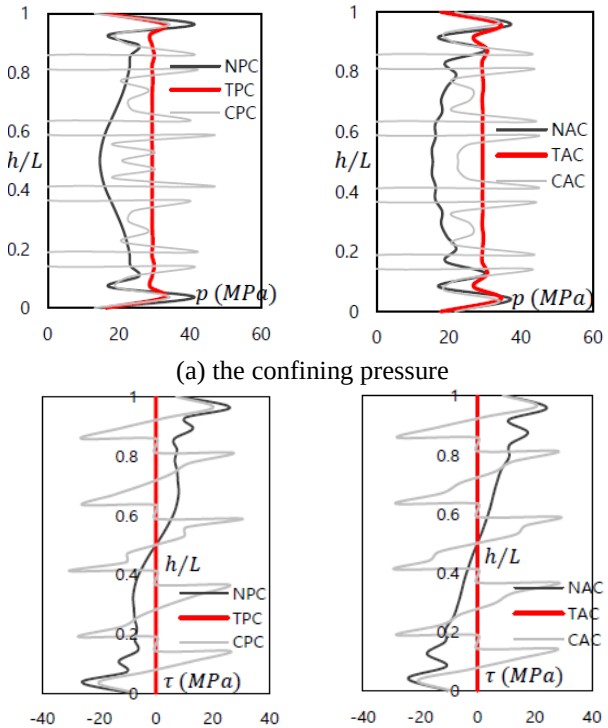

(a) the confining pressure

(b) the concrete core-steel tube interface shear stress

Fig. 5 Interface stresses at the peak strength for the active and passive specimens

should be noted that the curves associated with the lubricated specimens are not plotted here since the experimental results of the normal and lubricated specimens

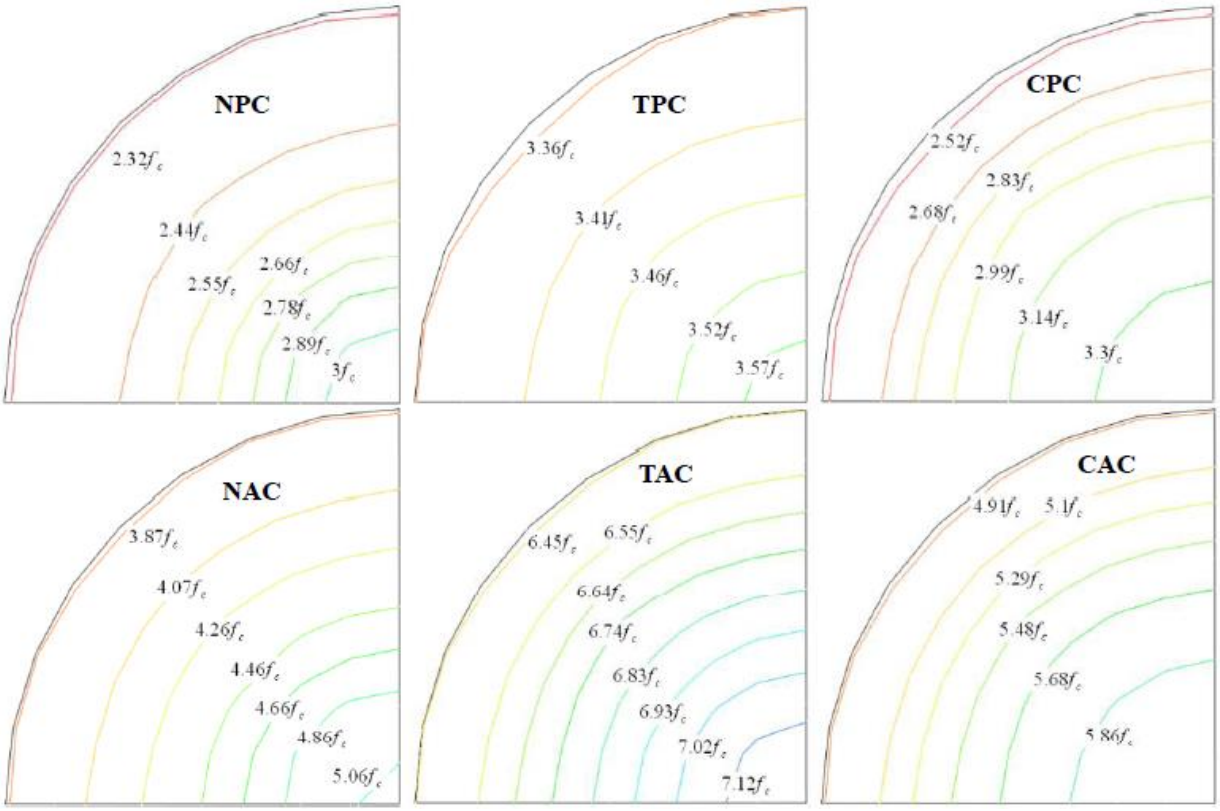

Fig. 6 The axial stress distribution in the concrete core at the peak strength for the active and passive specimens

are almost identical (Ghadami and Nematzadeh 2016). It is observed in Fig. 4 that by reducing or removing the shear stress from the concrete-steel interface in the active and passive specimens, the load-carrying capacity of the concrete core increases, such that in the talc-coated specimens, this trend is more salient with the elimination of the shear stress, with almost the entire applied load being carried by the concrete core. Moreover, reduction or elimination of the shear stress leads to a lower compressive load-carrying of the steel tube in the longitudinal direction as well as an increase in its confining pressure. The confining stress at peak point for the passively-confined circumferential-grooved and talc-coated specimens is 1.87 and 1.98, respectively, times as much as that for the passively-confined normal specimens. These values are 1.78 and 4.11 for corresponding active specimens. The ratio of confining pressure in the active state to that in the passive state for the circumferential-grooved, talc-coated, and normal specimens is 1.01, 2.20, and 1.06, respectively.

As can be seen in Table 2, the change in the shear stress condition has a negligible effect on the peak compressive strength of the passive specimens, while this is not the case for the active specimens, with a significant increase up to 28% following the elimination or reduction of the shear stress relative to the actively-confined normal concrete. The values of 1.76, 1.96, and 1.53 are obtained for the ratio of the peak compressive strength of the active state to that of the passive one in the circumferential-grooved, talc-coated, and normal specimens, respectively. These results suggest that the load-carrying portion of the concrete core, the confining pressure, and the peak compressive strength increase significantly by prestressing the column and removing the concrete-steel interface shear stress.

5.2 Interface stresses

The confining pressure applied to the concrete core at peak strength along the column height for the active and passive specimens is illustrated in Fig. 5(a), where h denotes the distance from the steel tube top end. As can be seen, the confining pressure for the actively- and passively-confined circumferential-grooved and normal specimens has the maximum value at the two column ends, and by moving toward the mid-height of the column, it decreases to its minimum value. Since the longitudinal stress is the maximum at the mid-height and the hoop stresses have their minimum values at the mid-height accordingly, a smaller confining pressure develops at the mid-height. Notice that since the longitudinal stress of the steel tube in the actively- and passively-confined talc-coated specimens is zero and its hoop stress is the maximum and uniform, the confining pressure remains constant along the tube length while possessing the highest value compared to the other specimens.

Fig. 5(b) shows the concrete-steel interface shear stress at the peak strength for the active and passive specimens. Note that the shear stress in the talc-coated specimen is zero due to the lack of shear stress transfer between the concrete core and the steel tube. Since the load transfer from the concrete core to the steel tube in the normal specimens starts from the ends, the highest relative axial displacement between the concrete and steel occurs there, and decreases

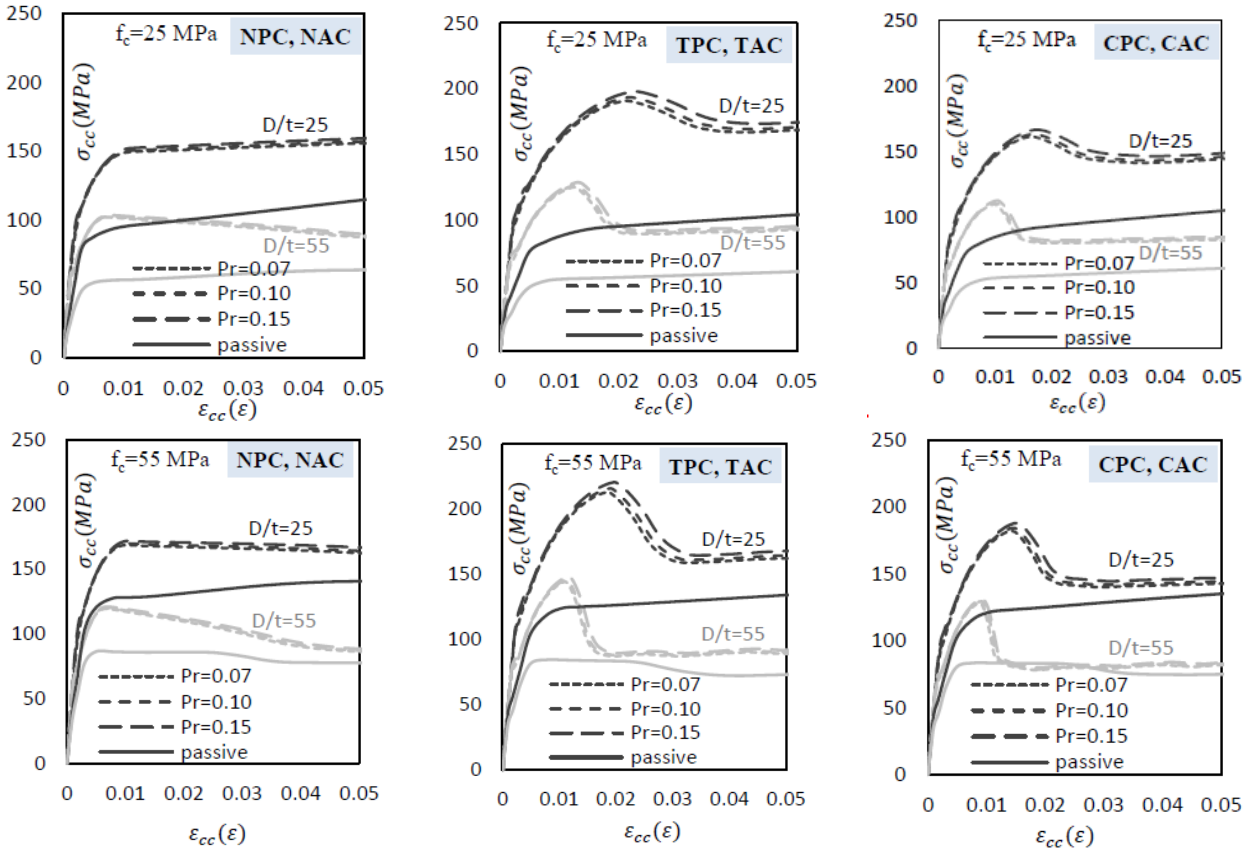

Fig. 7 The axial stress-strain curves with different D/t, f_c, and P_r values for the active and passive specimens

gradually as the distance increases. Hence, the shear stress in the normal specimens having active and passive confinement is the maximum at the end regions, and at the mid-height, it becomes zero considering the symmetry and the lack of slip. The same trend is observed for each ring of the active and passive circumferential-grooved specimens.

5.3 Longitudinal stress distribution in cross-section

In Fig. 6, the axial stress distribution in the concrete core at the peak strength for the active and passive specimens in the normal, talc-coated, and circumferential-grooved groups is demonstrated. From the figure, it can be found that the axial stress distribution is non-uniform throughout the concrete core, with a gradual decrease as the distance from the concrete center increases. However, this non-uniformity is more salient in the normal specimens in relation to the talc-coated and circumferential-grooved specimens. Additionally, it is also found out from the figure that reducing or eliminating the shear stress leads to the increasing longitudinal stress in the concrete core, meaning that in the talc-coated and circumferential-grooved specimens, the applied load is carried by the concrete core, and the steel tube plays only a confining role.

6. Parametric study

Following the verification of the finite element model, the effect of variations in the concrete compressive strength, steel tube wall thickness, and prestressing level on the compressive behavior of the STCC columns was investigated. A total of 48 passive specimens and 36 active specimens in the three groups of circumferential-grooved, talc-coated, and normal, the properties of which is given in Table 3, were analyzed in the parametric study.

6.1 The axial stress-strain curve of composite section

Fig. 7 shows the axial stress-strain curve of the composite section with different D/t, f_c, and P_r values for the active and passive circumferential-grooved, talc-coated, and normal specimens. With respect to the figure, at a given D/t and f_c, all active curves sit above the passive ones, which is more obvious for the lower-strength concretes. Moreover, as can be seen in the figure, the linear region of the active specimens is much bigger than that of the passive specimens, indicating that prestressing by the current method is capable of significantly improving the compressive behavior of the STCC columns under any concrete-steel interface shear stress condition. However, increasing the prestressing level, as shown in the figure, has a negligible effect on the compressive behavior of the STCC columns. Additionally, as D/t increases, the stress at a given strain decreases in all the active and passive specimens. For the active specimens, as the concrete compressive strength increases, so does the stress values; however, the curve experiences a drop with a sharper gradient at the peak point.

Table 3 The specifications of the active and passive specimens in the parametric study and the FEA results

Specimen	Type of confinement	D/t	t (mm)	L_c (mm)	L_s (mm)	f_c (MPa)	P_r	$fcc_{(N)}$ (MPa)	$fcc_{(T)}$ (MPa)	$fcc_{(C)}$ (MPa)	$\frac{f_{cc(T)}}{f_{cc(N)}}$	$\frac{f_{cc(C)}}{f_{cc(N)}}$
P1	Passive	25	2.41	140	150	25	-	97.8	95.1	92.4	0.97	0.94
P2	Passive	25	2.41	140	150	35	-	108.5	105.9	103.6	0.98	0.95
P3	Passive	25	2.41	140	150	45	-	118.7	116.1	114.1	0.98	0.96
P4	Passive	25	2.41	140	150	55	-	128.5	125.9	124.0	0.98	0.97
P5	Passive	35	1.68	140	150	25	-	77.6	77.8	76.0	1.00	0.98
P6	Passive	35	1.68	140	150	35	-	87.9	88.2	86.6	1.00	0.98
P7	Passive	35	1.68	140	150	45	-	97.9	98.1	96.7	1.00	0.99
P8	Passive	35	1.68	140	150	55	-	107.5	107.5	106.2	1.00	0.99
P9	Passive	45	1.29	140	150	25	-	65.4	65.6	64.3	1.00	0.98
P10	Passive	45	1.29	140	150	35	-	75.6	75.8	74.6	1.00	0.99
P11	Passive	45	1.29	140	150	45	-	85.4	85.5	84.4	1.00	0.99
P12	Passive	45	1.29	140	150	55	-	94.9	94.7	93.7	1.00	0.99
P13	Passive	55	1.05	140	150	25	-	56.6	55.7	54.6	0.98	0.96
P14	Passive	55	1.05	140	150	35	-	66.7	65.6	64.7	0.98	0.97
P15	Passive	55	1.05	140	150	45	-	76.3	75.1	74.2	0.98	0.97
P16	Passive	55	1.05	140	150	55	-	85.6	83.9	83.2	0.98	0.97
A1	Active	25	2.41	124	134	25	0.07	149.6	190.5	161.5	1.27	1.08
A2	Active	25	2.41	124	134	25	0.10	150.7	192.7	163.5	1.28	1.09
A3	Active	25	2.41	124	134	25	0.15	152.3	196.3	166.9	1.29	1.10
A4	Active	25	2.41	124	134	55	0.07	168.4	213.1	182.1	1.27	1.08
A5	Active	25	2.41	124	134	55	0.10	169.7	216.0	184.2	1.27	1.09
A6	Active	25	2.41	124	134	55	0.15	171.7	220.6	187.8	1.29	1.09
A7	Active	55	1.05	124	134	25	0.07	101.9	125.0	109.8	1.23	1.08
A8	Active	55	1.05	124	134	25	0.10	102.4	126.4	110.9	1.23	1.08
A9	Active	55	1.05	124	134	25	0.15	103.3	128.7	112.7	1.25	1.09
A10	Active	55	1.05	124	134	55	0.07	119.3	144.5	128.4	1.21	1.08
A11	Active	55	1.05	124	134	55	0.10	119.9	146.0	129.5	1.22	1.08
A12	Active	55	1.05	124	134	55	0.15	120.8	148.4	131.5	1.23	1.09

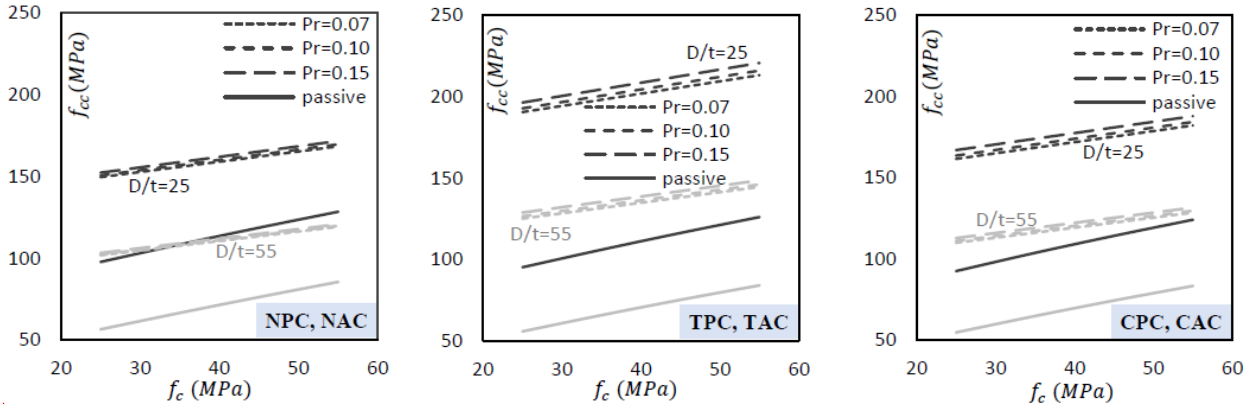

Fig. 8 The peak compressive strength vs. concrete compressive strength for the active and passive specimens with different values of D/t and P_r

6.2 The peak compressive strength

Fig. 8 illustrates the peak compressive strength vs. concrete compressive strength curves for the active and passive specimens with different values of D/t and P_r. Moreover, the numerical values of the peak compressive strength for the active and passive specimens are given in Table 3. It is found from Fig. 8 and Table 3 that the peak

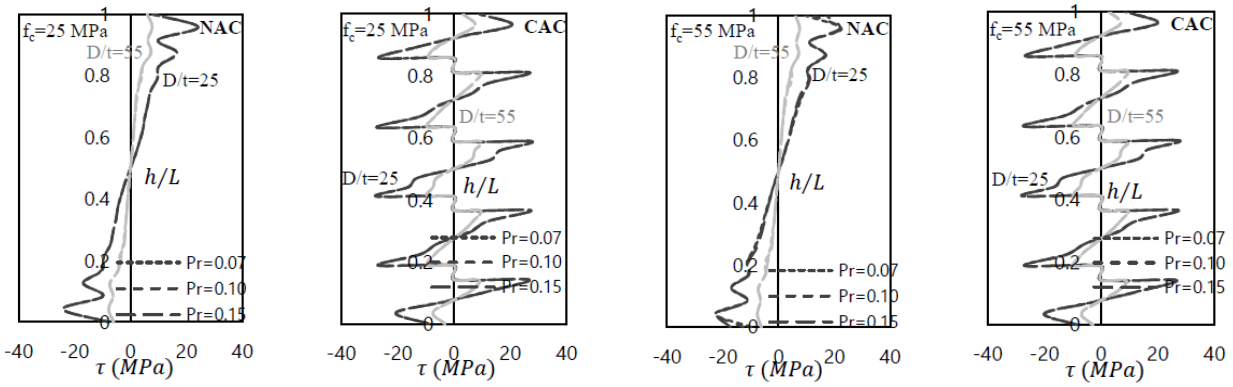

Fig. 9 The shear stress between the concrete core and the steel tube at the peak strength in the active specimens with different values of D/t, f_c, and P_r

compressive strength of the active and passive specimens increases as the concrete compressive strength increases under any interface shear stress condition, with the trend becoming more evident as D/t increases. The peak compressive strength of the active and passive specimens under different shear stress conditions decreases with increasing D/t. In the passive specimens, this trend is more evident for lower concrete strength values, while in the active specimens, changes in the concrete strength have little influence on the decreasing trend of the peak compressive strength. Furthermore, the prestressing ratio negligibly affects the peak compressive strength of the active specimens.

Generally, the increase in the peak compressive strength of the passive specimens is significantly higher than that of the active ones. This is clearly seen from the slope of the curves. The ratio of the peak strength of the talc-coated specimens to that of the normal ones ($f_{cc(T)}/f_{cc(N)}$) and the ratio of the peak strength of the circumferential-grooved specimens to that of the normal ones ($f_{cc(C)}/f_{cc(N)}$) are both about 1 for the passive specimens, while for the active specimens, they are about 1.25 and 1.1, respectively. This indicates that, unlike the active specimens, the peak strength of the passive specimens is not under the influence of the condition of the shear stress.

6.3 The interface shear stress

In Fig. 9, the shear stress at the interface between the concrete core and the steel tube at the peak strength along the height of the active specimens is shown. It is observed in the figure that increasing the concrete compressive strength as well as prestressing level has a small influence on the interface shear stress in the actively-confined circumferential-grooved and normal specimens. However, as D/t increases, the interface shear stress decreases. This is because decreasing the steel tube wall thickness leads to a pressure reduction at the concrete-steel interface thus a reduction of the friction force is resulted.

6.4 Comparing normal and circumferential-grooved specimens with the same steel volume

Since the volumes of steel used in the circumferential-grooved and normal specimens in the work of Ghadami and Nematzadeh (2016) are not the same, it will be better to investigate the effect of the circumferential grooving of the steel tube on the column compressive behavior with the same steel volume as that of the normal specimen. To do so, the confining tube's volumetric increase in the circumferential-grooved specimen is modeled as an increase in the tube wall thickness (the steel tube wall thickness increases from 2.50 to 3.04 mm). The stress-strain curves of the active and passive normal and circumferential-grooved specimens with the same volume of steel are shown in Fig. 10. The peak compressive strength of the active and passive circumferential-grooved specimens is about 15% and 5%, respectively, more than that of the active and passive normal specimens, which results from the reduction of the concrete-steel interface shear stress and thus the increase of confining pressure. Additionally, as can be seen in Fig. 10, the difference between the two curves at high strains becomes more noticeable.

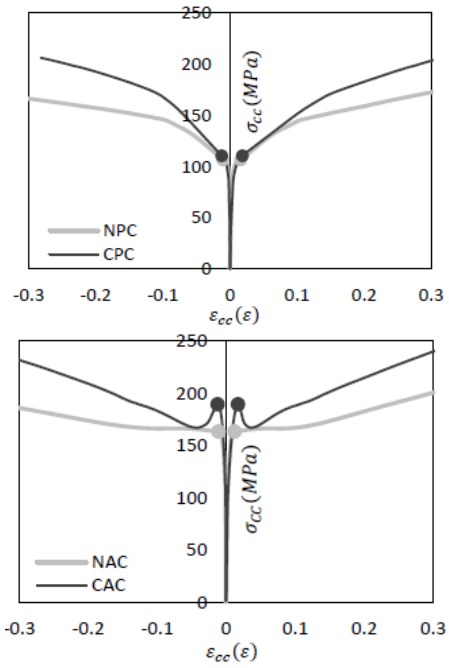

Fig. 10 Comparison between the stress-strain curves of the active and passive normal and circumferential-grooved specimens with the same volume of the steel

7. Conclusions

In this study, 3D nonlinear finite element models were developed to investigate the effect of the concrete-steel interface shear stress in the STCC columns with active and passive confinement in the four groups, i.e., the circumferential-grooved, lubricated, talc-coated, and normal specimens. The inelastic properties of the steel and concrete materials, the effect of concrete confinement, steel tube prestressing level, and compressed concrete properties were all taken into account in the models. The composite column strength as well as its stress-strain relationship were then predicted using the finite element models, and were subsequently compared with the experimental results. Comparing the experimental results with the numerical ones showed that the proposed model is capable of accurately predicting the behavior of the STCC columns with active and passive confinement. The verified finite element model was employed in order to study the effect of shear stress on the compressive behavior of the actively- and passively-confined columns, and thus the following conclusions can be drawn:

• Change in the shear stress condition has a negligible effect on the peak compressive strength of the passive specimens, whereas reduction or elimination of the shear stress results in an increase in the peak strength of the active specimens.

• By decreasing or eliminating the interface shear stress, the longitudinal stress of the steel tube experiences a significant decrease along the tube length while the hoop stress and the confining pressure increase.

• Prestressing using the present method allows for significant improvement of the compressive behavior of the STCC columns under any given shear stress condition; however, increasing the prestressing level negligibly affects that.

• As the steel tube outer diameter-to-wall thickness ratio increases, the axial stress values decrease for all the active and passive specimens, while its values increase with increasing concrete compressive strength.

• The interface shear stress in the circumferential-grooved and normal specimens decreases as the steel tube outer diameter-to-wall thickness ratio increases, while the effect of an increase in the concrete compressive strength as well as prestressing level on the interface shear stress is negligible.

• In the same steel volume, the compressive strength of the circumferential-grooved specimen under active and passive confinement is significantly greater than that of the corresponding normal specimen.

References

ACI 318M (2008), *Building Code Requirements for Structural Concrete and Commentary*, American Concrete Institute, U.S.A.

Chen, Q. and Andrawes, B. (2012), "3D finite element modeling to study the behavior of shape memory alloy confined concrete", *Proceedings of the 15th World Conference on Earthquake Engineering*, Lisbon, Portugal, September.

Ghadami, J. and Nematzadeh, M. (2016), "Effect of bond shear stress on compressive behaviour of steel tube-confined concrete with active and passive confinement", *Eur. J. Environ. Civil Eng.*

Gupta, P.K., Verma, V.K., Khaudhair, Z.A. and Singh, H. (2015), "Effect of tube area on the behavior of concrete filled tubular columns", *Comput. Concrete*, **15**(2), 141-166.

Haghinejad, A. and Nematzadeh, M. (2016), "Three-dimensional finite element analysis of compressive behavior of circular steel tube-confined concrete stub columns by new confinement relationships", *Lat. Am. J. Sol. Struct.*, **13**, 916-944.

Hibbitt, Karlson & Sorensen Inc (2003), *ABAQUS/Standard User's Manual*, Version 6.12 Pawtucket, RI, U.S.A.

Hu, H.T. and Schnobrich, W.C. (1989), "Constitutive modeling of concrete by using non-associated plasticity", *J. Mater. Civil Eng.*, **1**(4), 199-216.

Hu, H.T., Huang, C.S., Wu, M.H. and Wu, Y.M. (2003), "Nonlinear analysis of axially loaded concrete-filled tube columns with confinement effect", *J. Struct. Eng.*, **129**(10), 1322-1329.

Johansson, M. and Gylltoft, K. (2002), "Mechanical behaviour of circular steel-concrete composite stub columns", *J. Struct. Eng.*, **128**(8), 1073-1081.

Mander, J.B., Priestley, M.J.N. and Park, R. (1988), "Theoretical stress-strain model for confined concrete", *J. Struct. Eng.*, **114**(8), 1804-1826.

Moghaddam, H., Samadi, M. and Pilakoutas, K. (2010), "Compressive behavior of concrete actively confined by metal strips, part B: Analysis", *Mater. Struct.*, **43**, 1383-1396.

Nemati, S.T. (2006), "Effect of active confinement on concrete behavior", M.S. Dissertation, University of Mazandaran.

Nematzadeh, M. and Haghinejad, A. (2017), "Analysis of actively-confined concrete columns using prestressed steel tubes", *Comput. Concrete*, **19**(5), 477-488.

Nematzadeh, M. and Naghipour, M. (2012), "Compressive strength and modulus of elasticity of freshly compressed concrete", *Constr. Build. Mater.*, **34**, 476-485.

Nematzadeh, M., Naghipour, M., Jalali, J. and Salari, A. (2017), "Experimental study and calculation of confinement relationships for prestressed steel tube-confined compressed concrete stub columns", *J. Civil Eng. Manage.*, **23**(6), 699-711.

Qi, H.T., Guo, L.H., Liu, J.P., Gan. D. and Zhang, S.M. (2011), "Axial load behavior and strength of tubed steel reinforced-concrete (SRC) stub columns", *Thin-Wall. Struct.*, **49**(9),1141-1150.

Richart, F.E., Brandzaeg, A. and Brown, R.L. (1928), *A Study of the Failure of Concrete under Combined Compressive Stresses*, University of Illinois Engineering Experimental Station, Champaign, Illinois, U.S.A.

Saenz, LP. (1964), "Discussion of 'equation for the stress-strain curve of concrete' by P. Desayi and S. Krishnan", *ACI J.*, **61**, 1229-1235.

Schneider, S.P. (1998), "Axially loaded concrete-filled steel tubes", *J. Struct. Eng.*, **124**(10), 1125-1138.

Shraideh, M.S. and Aboutaha, R.S. (2013), "Analysis of steel-GFRP reinforced concrete circular columns", *Comput. Concrete*, **11**(4), 351-364.

Tao, Z., Wang, Z.B. and Yu, Q. (2013), "Finite element modelling of concrete-filled steel stub columns under axial compression", *J. Constr. Steel Res.*, **89**, 121-131.

Yu, Q., Tao, Z., Liu, W. and Chen, Z.B. (2010), "Analysis and calculations of steel tube confined concrete (STCC) stub columns", *J. Constr. Steel Res.*, **66**, 53-64.

CC